Exciton Localization in Two-Dimensional Semiconductors Through Modification of the Dielectric Environment

A Preprint

● **Kelly Y. Muñoz-Gómez** ● **Hanz Y. Ramírez-Gómez** *
Grupo de Física Teórica y Computacional & Grupo QUCIT,
Escuela de Física, Universidad Pedagógica y Tecnológica de Colombia (UPTC),
Tunja 150003, Boyacá, Colombia.

November 4, 2024

Abstract

Monolayer semiconductors, given their thickness at the atomic scale, present unique electrostatic environments due to the sharp interfaces between the semiconductor film and surrounding materials. These interfaces significantly impact both the quasiparticle band structure and the electrostatic interactions between charge carriers.

A key area of interest in these materials is the behavior of bound electron-hole pairs (excitons) within the ultra-thin layer, which plays a crucial role in its optoelectronic properties.

In this work, we investigate the feasibility of generating potential traps that completely confine excitons in the thin semiconductor by engineering the surrounding dielectric environment. By evaluating the simultaneous effects on bandgap renormalization and modifications to the strength of the electron-hole Coulomb-interaction, both associated to the modulation of the screening by the materials sandwiching the monolayer, we anticipate the existence of low-energy regions in which the localization of the exciton center of mass may be achieved.

Our results suggest that for certain dielectric configurations, it is possible to generate complete discretization of exciton eigenenergies in the order of tens of meV. Such quantization of energy levels of two-dimensional excitons could be harnessed for applications in new-generation optoelectronic devices, which are necessary for the advancement of technologies like quantum computing and quantum communication.

Keywords Confined Excitons · 2D Heterostructures · ; Dielectric Modulation.

1 Introduction

Over the past two decades, two-dimensional (2D) semiconductors have garnered significant attention due to their exceptional optical and electronic properties, which differ fundamentally from those of their bulk counterparts [1, 2]. These materials, characterized by their atomic-scale thickness, exhibit charge carriers strongly confined in a plane, leading to unique excitonic effects and tunable energy band structures [3]. A particularly compelling feature of 2D semiconductors is their ability to host excitons whose properties can be precisely controlled through external factors such as strain, electric fields, or, as explored in this study, the surrounding dielectric environment [4, 5, 6]. This level of control has opened up new possibilities for applications in fields such as quantum-light generation and single-particle optoelectronic devices.

Experimentally, 2D materials have been widely explored as light-emitting sources [7]. Recent progresses in the fabrication, characterization and application of 2D heterostructures have shown how these engineered structures,

---

* hanz.ramirez@uptc.edu.co

typically comprising materials like graphene, hexagonal boron nitride (hBN) and transition metal dichalcogenides (TMDCs), unlock new properties and applications beyond those of their individual components [8, 9]. Furthermore, substantial advancements have been made in the synthesis of van der Waals heterostructures, with their applications extending to electronics, sensing, optoelectronics and energy conversion [10, 11].

It is well established that the dielectric environment surrounding a 2D semiconductor plays a critical role in modulating the Coulomb interaction between electron and hole (e-h) pairs [12, 13, 14]. In homogeneous environments, the e-h interaction is primarily governed by the relationship between the dielectric constants of the semiconductor and the surrounding materials [15, 16, 17, 18]. However, the presence of non-uniform dielectric surroundings along the in-plane directions has been shown to significantly alter this interaction, resulting in phenomena such as changes in dielectric screening, local bandgap renormalization, and enhanced carrier confinement [12, 19, 20]. These modulations are expected to affect exciton binding energies and radiative lifetimes, both of which are crucial for designing efficient optoelectronic devices.

In low-dimensional semiconductors, bandgap renormalization arises from changes in field screening across interfaces [21, 22]. This effect can be significant when there is a strong contrast between the dielectric properties of the semiconductor nanostructure and the materials surrounding it.

Additionally, the strength of the electrostatic interaction between confined carriers is sensitive to the dielectric environment and can be substantially altered when the polarizabilities of the involved materials differ significantly [23, 12].

In this work, we explore the interplay between bandgap renormalization and changes in the exciton binding energy in a 2D semiconductor, specifically considering the effects of inhomogeneities in the dielectric surroundings along the in-plane directions. We begin by introducing the system under consideration and the proposed Hamiltonian used to study the impact of the modified dielectric environment. Next, we present numerical results for a monolayer surrounded by two inhomogeneous slabs. Finally, we analyze the outcomes and provide key conclusions.

2   System Hamiltonian

The specific system under study consists of a semiconductor monolayer sandwiched between two slabs of a material with dielectric constant ε_{II}, each of them with a circular hole of diameter D. Such a cylindrical cavity is considered filled with another material of dielectric constant ε_I (which could be air, i.e. $\varepsilon_I = 1$). This configuration is depicted in figure 1, where a perspective and a side view are provided.

Figure 1(b) illustrates two distinct regions within the 2D semiconductor: region I ($0 \leq \rho < D/2$) and region II ($D/2 \leq \rho < \infty$), defined by the boundaries of the dielectric environment.

For e-h pairs in the 2D semiconductor, we will use the standard transformation of coordinates for the center-of-mass ($\boldsymbol{R}$) and relative ($\boldsymbol{r}$) positions [24, 25]. The origin of coordinates is taken vertically at mid-height of the 2D semiconductor, and horizontally at the center of the hollow in the dielectric slabs (see figure 1). Due to the atomic-scale thickness of the semiconductor, where the excitons are confined, we set $Z = z = 0$ for both the vertical e-h center-of-mass and the relative positions. In the side view shown in figure 1(b), ρ stands for the magnitude of the in-plane component of the relative-position vector.
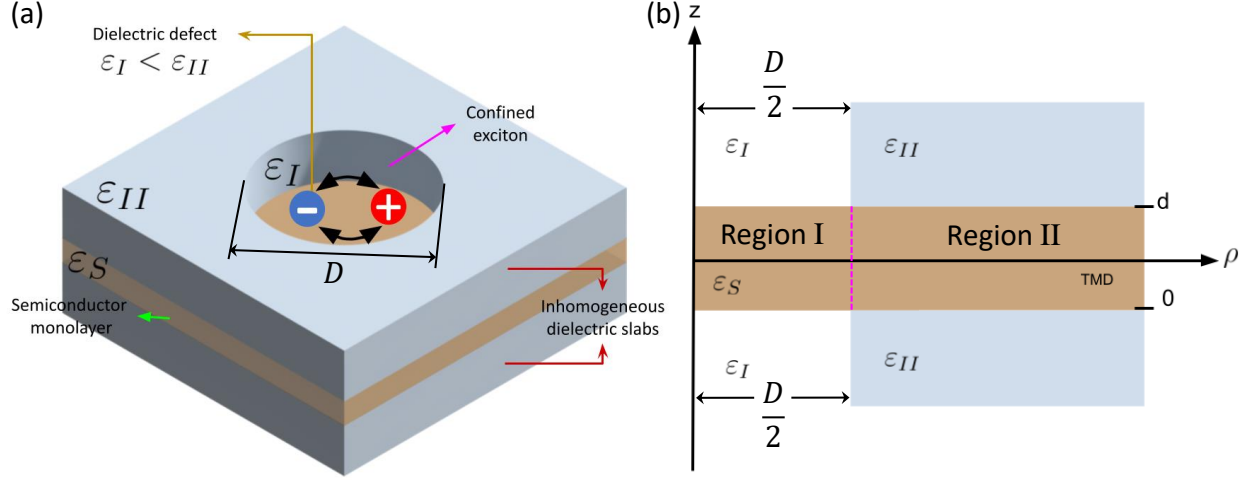
Figure 1: (a) Schematic of the studied heterostructure. (b) Side view of the Inhomogeneous-dielectric/2D-Semiconductor/Inhomogeneous-dielectric stack. ρ is the in-plane component of the relative position.

To write a Hamiltonian for this system, three assumptions are made: i) The exciton radius r_X is much smaller than D, ii) The electron, hole and e-h center of mass are always in the same region, and iii) The electron and hole effective masses are the same in regions I and II.

The first two assumptions are based on the fact that the typical exciton radius in 2D transition metal dichalcogenides is in the order of angstroms [26], while we will consider cylindrical cavities with diameters in the order of several nanometers [27]. The third assumption is reasonable because the in-plane effective masses of carriers inside the thin semiconductor are expected to mainly depend on the crystalline structure of that material, instead of being dominated by the dielectrics above and below it [28].

Based on the above assumptions, we describe the position-represented Hamiltonian in terms of a Heaviside function $h(x)$ ($h(x) = 0$ for $x < 0$ and $h(x) = 1$, otherwise), according to

$$H = -\frac{\hbar^2}{2M}\nabla_{\mathbf{R}}^2 - \frac{\hbar^2}{2\mu}\nabla_{\mathbf{r}}^2 + [1 - h(R - D)] \times \left[E_B^I + V_I^{e-h}(\boldsymbol{r})\right] + h(R - D) \times \left[E_B^{II} + V_{II}^{e-h}(\boldsymbol{r})\right], \quad (1)$$

where R is the magnitude of the center of mass position, $\nabla_{\mathbf{R}}$ and $\nabla_{\mathbf{r}}$ are correspondingly the Laplacians respect to the center of mass and relative positions, while M and μ denote the total and reduced e-h masses, respectively. E_B^I and $V_I^{e-h}(\boldsymbol{r})$ (E_B^{II} and $V_{II}^{e-h}(\boldsymbol{r})$) are respectively, the quasiparticle bandgap and e-h Coulomb potential in region I (region II). Along this work we will consider only the direct part of the Coulomb interaction and neglect the exchange component, since in 2D semiconductors, the typical energy scale of the former has been shown more than one order of magnitude larger than the latter [2, 29].

"Bandgap renormalization" is an observed effect associated to changes in the dielectric environment [30, 31, 32, 33]. Because of it, the quantities E_B^I and E_B^{II} are expected to differ in an amount whose absolute value increases as the difference between dielectric constants of the 2D semiconductor and the locally surrounding dielectric raises.

To account for that renormalization effect, we use the model developed by Cho and Berkelbach in reference [6]. This formulation allows to obtain the change in the bandgap of a 2D sample respect to that of the bulk case, in terms of the difference between the involved dielectric constants. Accordingly, the bandgap modification ΔE_B^i is given by

$$\Delta E_B^i = \pm\frac{e^2}{2\varepsilon_S d}\left\{2\tanh^{-1}(L_{S,i}) - \ln\left(1 - L_{S,i}^2\right)\right\}, \quad (2)$$

where $L_{S,i}$ is a factor depending on the difference between the involved dielectric constants in each region, which reads

$$L_{S,i} = \frac{\varepsilon_S - \varepsilon_i}{\varepsilon_S + \varepsilon_i}, \quad (3)$$

3

with $i = I, II$.

The bandgap energy for reference E_B^{ref}, is that of the sandwiched semiconductor, but in bulk form. Respect to this value, the bandgap is renormalized according to the material surrounding the 2D semiconductor. Thus, if the material above and below that film is the semiconductor itself, there is not renormalization and the bandgap would obviously remain the same. In contrast, if the dielectric constant of the sandwiching material in region i is different to that of the semiconductor, the corresponding renormalized bandgap defined as

$$E_B^i \equiv E_B^{ref} + \Delta E_B^i, \tag{4}$$

may increase or decrease respect to the reference value, depending on whether such a difference $(\varepsilon_S - \varepsilon_i)$ is positive $(\Delta E_B^i > 0)$ or negative $(\Delta E_B^i < 0)$ [3].

Regarding the electrostatic interaction, because of the product with a function depending on the center of mass position $\boldsymbol{R}$, the e-h interaction potentials are not strictly separable. However, the abrupt form of the $h(R - D)$ function allows considering those potentials as depending exclusively on the magnitude of the relative position ρ within each of regions I and II.

For those potentials $V_i^{eh}(\rho)$ $(i = I, II)$, we use the form in terms of image charges, derived in references [17, 18]. This method permits to effectively incorporate the influence of the inhomogeneous dielectric environment on the electron-hole Coulomb interaction, as long as the e-h pair is assumed not to be very close to the boundary $R_x^2 + R_y^2 = D^2$. Such electrostatic potential, can be written in SI units as

$$V_i^{e-h}(\rho) = \frac{1}{4\pi\varepsilon_0}\left[\frac{e^2}{\varepsilon_S \rho} + 2\sum_{n=1}^{\infty}\frac{e^2 L_{Si}^{2n}}{\varepsilon_S\left\{\rho^2 + (2nd)^2\right\}^{1/2}} + 2L_{Si}\sum_{n=0}^{\infty}\frac{e^2 L_{Si}^{2n}}{\varepsilon_S\left\{\rho^2 + [(2n+1)d]^2\right\}^{1/2}}\right], \tag{5}$$

where d is the effective width of the 2D semiconductor (see figure 1(b)). We will refer to this potential as "Kumagai-Takagahara" (KT) potential.

Such a potential incorporates the effects of both, the top and bottom dielectric interfaces in quasi 2D systems, by means of an infinite but converging series of image charges [17, 18]. This potential was preferred over the more commonly used approach, known as Rytova-Keldysh (RK) potential, because the KT potential describes more accurately the e-h Coulomb interactions inside a 2D semiconductor surrounded by different types of dielectric materials. For instance, the RK potential assumes the limits $\rho \gg d$ and $\varepsilon_S \gg \varepsilon_i$, while the KT potential does not, which makes the latter applicable in a broader range of dielectric environments. Furthermore, it has been reported that the RK potential introduces some spurious effects due to its logarithmic asymptotic behavior for very short distances [6, 34].

Equations (1) through (5) provide a complete framework to study the net energetic effect produced by simultaneous changes in the bandgap and in the e-h electrostatic interaction, at the two different regions defined within the 2D semiconductor. Then, we can estimate the magnitude of the energy jump along the in-plane directions, that is expected to be generated because of the inhomogeneity of the slabs by which the semiconductor is sandwiched.

It is worth noting that the bandgap renormalization and the electrostatic modulation exhibit agreeing trends. i.e. for any configuration in which the bandgap increases, the e-h Coulomb potential is strengthened (its absolute value is enlarged). Similarly, in those configurations in which the bandgap decreases, the e-h Coulomb attraction is weakened.

The physical explanation for this behavior is depicted in figure 2. In the illustrated case (an interacting e-h pair), when the surrounding material is less polarizable than the semiconductor itself (figure 2(b)), the attractive electrostatic interaction in the 2D case is strengthened in comparison to the bulk case (figure 2(a)). On the contrary, if the surrounding material is more polarizable than the semiconductor, the screening by the surrounding material is more effective and then the interaction is weakened (figure 2(c)). Analogously happens with the repulsive interaction between electrons, which contributes to the bandgap size via the self-energy generated by the electron density in presence of the dielectric interfaces [35, 36].

Hence, for a region in which the 2D semiconductor is sandwiched by a material with dielectric constant smaller (bigger) than that of the semiconductor itself, the bandgap is expected to increase (decrease) as well as the magnitude of the exciton binding energy. Nevertheless, the energy variations associated to both of these effects are not necessarily equal. Then, there can be a net effect on the ground energy in each region.
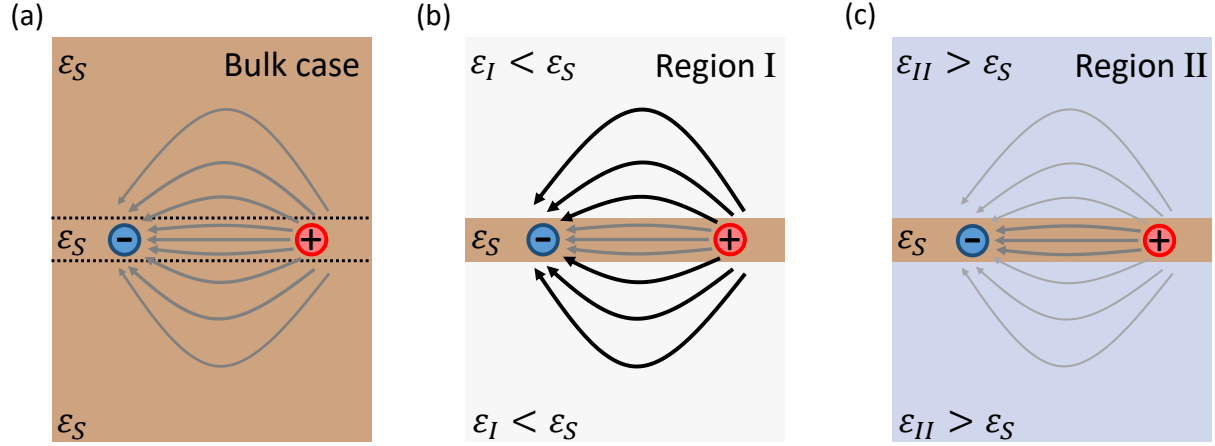
Figure 2: Depiction of the change in the electrostatic interaction depending on the dielectric surrounding. (a) A bulk sample, in which the boundaries of what would be the thin layer are represented by dashed lines. (b) The case in which the surrounding material has a smaller dielectric constant than the semiconductor itself (region I). The electrostatic interaction is strengthened. (c) As in (b) but the dielectric constant of the surrounding material is bigger (region II). In this case, the electrostatic interaction is weakened.

According to the Hamiltonian in equation (1), there will be two different energies for the ground state, depending on the position of the center of mass (whether in region I or in region II). If the ground energy for region I is lower than that for region II, region I would become a confinement area for excitons within the semiconductor (a well-like effective potential $V^{eff}(R)$ for the exciton center of mass). Otherwise, region I would turn into a region where the excitons are prevented to be located (a step-like effective potential $V^{eff}(R)$ for the exciton center of mass).

The ground energy for region i can be obtained from

$$E_G^i = E_B^i + E_0^i, \tag{6}$$

where $E_0^i \ (< 0)$ is the energy of the ground state of the exciton relative part, calculated by solving

$$-\frac{\hbar^2}{2\mu}\nabla_\rho^2 + V_i^{e-h}(\boldsymbol{\rho})\Psi_0^i(\boldsymbol{\rho}) = E_0^i\Psi_0^i(\boldsymbol{\rho}). \tag{7}$$

We take the difference between ground energies $\Delta E_G^{I-II} = E_G^I - E_G^{II}$ to be either, minus the deep of the potential well ($\Delta E_G^{I-II} < 0$) or the height of the potential step ($\Delta E_G^{I-II} > 0$), effectively "felt" by the exciton center of mass. This is schematized in figure 3.

(a)

$$V^{eff}(R)$$

(b)

$$V^{eff}(R)$$

$$|\Delta E_G^{I-II}|$$

$$R_x, R_y$$

$$\Delta E_G^{I-II} < 0$$

$$\Delta E_G^{I-II}$$
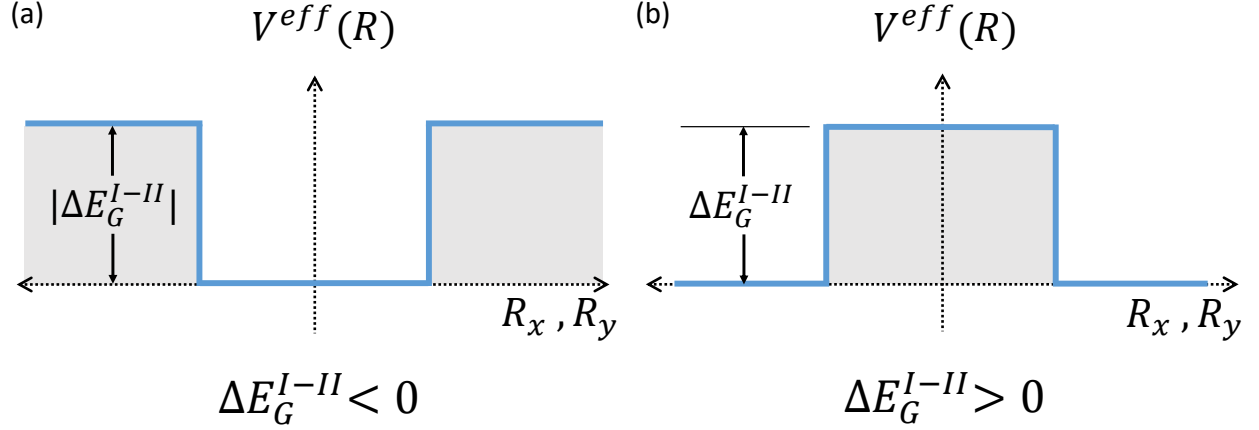
$$R_x, R_y$$

$$\Delta E_G^{I-II} > 0$$

Figure 3: (a) Effective potential well for the exciton center of mass, in the case $\Delta E_G^{I-II} < 0$ (b) Effective potential step for the exciton center of mass in the case $\Delta E_G^{I-II} > 0$

3 Numerical Results

In this section we study numerically three distinct configurations, corresponding to the 2D semiconductor sandwiched by three different materials in region II. In all the cases, the surrounding material in region I is taken as air ($\varepsilon_I = 1$), and for the dielectric constant of the ultra-thin semiconductor (assumed as WS$_2$) $\varepsilon_S = 14$ was used, taken as a representative value within the range reported for TMDC monolayers [37, 38]. Hence, the difference among the three studied cases is the dielectric constant ε_{II} of the material above and below region II (see figure 1(b)).

In **Case 1**, region II is assumed surrounded by a material with dielectric constant ($\varepsilon_{II} = 10 < \varepsilon_S$), i.e. a value approximated to that of Mica, a promising candidate for a 2D insulator [39, 40]. In **Case 2**, the assumed system is a bulk semiconductor with a transversal hole that does not go through the semiconductor monolayer ($\varepsilon_{II} = \varepsilon_S = 14$). This is an idealized case, useful as reference for the values of the quasiparticle bandgap and exciton binding energy related to the conventional Coulomb potential (figure 2(a), and first of the three terms in equation (5)). Finally, in **Case 3**, region II is assumed surrounded by a material with dielectric constant ($\varepsilon_{II} = 25$), representing Hafnium(IV) oxide (HfO$_2$), i.e. a material with very high dielectric constant [41, 42]. The values of the dielectric constants used in the calculations, are summarized in Table 1.

Dielectric constant	Case 1	Case 2	Case 3
ε_S	14	14	14
ε_I	1	1	1
ε_{II}	10	14	25

Table 1: Dielectric constants used in the numerical simulations.

Once these values are defined, we can proceed to obtain ΔE_G^{I-II} from equations (2), (4) and (6), for the three considered scenarios. To do that, it is necessary to solve numerically equation (8), which we do within the finite-elements framework, by means of the software COMSOL Multiphysics [43, 44, 45, 46].

To deal with the infinite series included in the KT potential, we carried out a convergence study that allowed us to truncate such a series after the first twenty terms.

The energy values obtained from our calculations are shown in Table 2, were the reference value E_B^{ref} (the energy bandgap for bulk WS$_2$), is included for the sake of completeness.

In figure 4, the information presented in Table 2 is graphically illustrated. There, the competing effects from bandgap renormalization and Coulomb-interaction modulation can be visualized. The **blue horizontal line** indicates the bandgap energy when there is only semiconductor material, with a dielectric constant ε_S. The **magenta vertical lines** represent the bandgap renormalization energies E_B^i calculated using equation (5), while the **orange vertical lines** show in each region the ground-state energies for the relative exciton part E_0^i, calculated from equation (8) by using the KT potential. The **red lines** highlight the energy difference between the two effects for each studied case (ΔE_G^{I-II}).

Energy (eV)	Case 1	Case 2	Case 3
E_B^{ref}	1,350	1,350	1,350
E_B^I	1,695	1,695	1,695
E_B^{II}	1,381	1,350	1,307
E_0^I	-0,637	-0,637	-0,637
E_0^{II}	-0,129	-0,092	-0,049
ΔE_G^{I-II}	0.194	0.200	0.201

Table 2: Energy values obtained for the three scenarios under study (eV). The value E_B^{ref} is taken for bulk WS$_2$ from references [47, 48]
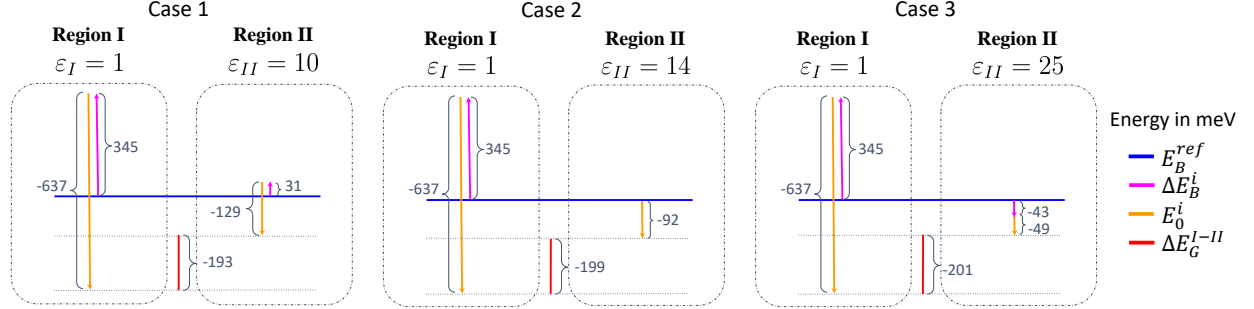

Figure 4: Visualization of the competing effects from bandgap renormalization and modulated Coulomb interaction. E_B^{ref} (blue line), ΔE_B^i (magenta line), E_0^i (orange line) and ΔE_G^{I-II} (red line).

The red lines in figure 4, highlight the net effect of the changes in dielectric environment between region I and II. For the three considered scenarios, the observed behavior is similar: a potential well is formed for the exciton center of mass, with an effective energy barrier (ΔE_G^{I-II}) in the order of few hundreds of meV. From this, it can be expected that in any of these cases, excitons are much more likely to be located in region I than in region II (figure 3(a)).

If the dielectric constants of the materials defining regions I and II would be exchanged, a potential step around the coordinate origin would be formed in all three cases (figure 3(b)), and excitons would be repelled from region I, generating an exciton-free region within the 2D semiconductor.

To estimate for a given D, the energy scale in which the center-of-mass eigenenergies would be discretized as consequence of the effectively generated potential well, we need to solve the eigenvalue equation

$$-\frac{\hbar^2}{2M}\nabla_{\mathbf{R}}^2 + V^{eff}(\mathbf{R})\phi_n(\mathbf{R}) = E_0^C\phi_n(\mathbf{R}), \qquad (8)$$

where $V^{eff}(\mathbf{R}) = |\Delta E_G^{I-II}| \times h(R-D)$ ($V^{eff}(\mathbf{R}) = 0$ if $R < D$ and $V^{eff}(\mathbf{R}) = |\Delta E_G^{I-II}|$ otherwise), and E_0^C are the discretized energies related to the center-of-mass confinement. To obtain those values, we suppose holes in the dielectric slabs of diameter $D = 5$ nm, and again find numerical solutions by means of the finite element method, as implemented in references [49, 50, 51, 52].

The obtained values for the first three eigenenergies in each of the studied configurations are shown in Table 3. E_1^C and E_2^C are degenerated in all cases because of the axial symmetry of the system.

Energy levels	Case 1	Case 2	Case 3
E_0^C	19,74	19,82	19.83
$E_{1,2}^C$	49.76	49.98	50
E_3^C	88.62	89.06	89.11

Table 3: Discretized center-of-mass energies (meV). $E_{1,2}$ are degenerated in each case.

The values presented in Table 3, show that the energy discretization would be very similar in any of the three considered cases, being the exciton localization almost insensitive to the specific type of dielectric used in region II.

7

The obtained energy values, suggest a significant discretization of levels, big enough for eventual experimental observation, even without the use of cryogenic setups. Further work needs to be done, for finding additional configurations that would lead to similar discretization but with larger inhomogeneities in the dielectric environment, so that the experimental realization is facilitated.

Such a discretization, of the order of tens of meV, seems advantageous for diverse application that would benefit of combining the attractive properties of 2D materials and zero-dimensional nanostructures.

4 Conclusions

We have studied the possibility of localizing exciton in 2D semiconductors, by modifying the dielectric environment. The obtained numerical results demonstrated that inhomogeneities in the dielectric environment may result in complete discretization of exciton energies.

Such quantization of energy levels, indicates the possibility of creating quantum dots in an ultra-thin semiconductor film. This offers valuable insight into how exciton confinement can be achieved through dielectric modulation.

These findings are expected to contribute to advancements in the development of artificial atoms with tunable properties, which are promising for the fabrication of high-performance quantum light sources, that are in turn, essential for the development of photon-based quantum technologies, such as quantum communication and quantum computing.

References cited

[1] S. Ayari, A. Smiri, A. Hichri, S. Jaziri, and T. Amand, "Radiative lifetime of localized excitons in transition metal dichalcogenides," *Physical review. B, Condensed matter*, vol. 98, 03 2018.

[2] G.-H. Peng, P.-Y. Lo, W.-H. Li, Y.-C. Huang, Y.-H. Chen, C.-H. Lee, C.-K. Yang, and S.-J. Cheng, "Distinctive signatures of the spin- and momentum-forbidden dark exciton states in the photoluminescence of strained wse 2 monolayers under thermalization," *Nano Letters*, vol. 19, 03 2019.

[3] N. Gauriot, A. Ashoka, J. Lim, S. See, J. Sung, and A. R. Ananth, "Direct imaging of carrier funneling in a dielectric engineered 2d semiconductor," *ACS Nano*, vol. 18, 12 2023.

[4] A. Hichri, I. Amara, S. Ayari, and S. Jaziri, "Exciton center-of-mass localization and dielectric environment effect in monolayer ws 2," *Journal of Applied Physics*, vol. 121, p. 235702, 06 2017.

[5] A. Smiri, T. Amand, and S. Jaziri, "Optical properties of exciton in two-dimensional transition metal dichalcogenide nanobubbles," *The Journal of chemical physics*, 03 2021.

[6] Y. Cho and T. Berkelbach, "Environmentally-sensitive theory of electronic and optical transitions in atomically-thin semiconductors," *Physical Review B*, vol. 97, 09 2017.

[7] J. Pu and T. Takenobu, "Monolayer transition metal dichalcogenides as light sources," *Advanced Materials*, vol. 30, p. 1707627, 06 2018.

[8] H. Wang, F. Liu, Z. Fang, W. Zhou, and Z. Liu, "Two-dimensional heterostructures: Fabrication, characterization, and application," *Nanoscale*, vol. 6, 08 2014.

[9] Q. Junlei, Z. Wu, W. Wang, K. Bao, L. Wang, J. Wu, C. Ke, Y. Xu, and Q. He, "Fabrication and applications of van der waals heterostructures," *International Journal of Extreme Manufacturing*, vol. 5, 04 2023.

[10] Z. Wang, B. Xu, S. Pei, J. Zhu, T. Wen, C. Jiao, J. Li, M. Zhang, and J. Xia, "Recent progress in 2d van der waals heterostructures: fabrication, properties, and applications," *Science China Information Sciences*, vol. 65, 09 2022.

[11] V. H. Nguyen, M. Kim, C. T. Nguyen, M. Suleman, N. Cong, N. Nasir, M. Rehman, H. Park, S. Lee, S. Kim, S. Kumar, and Y. Seo, "Fast fabrication technique for high-quality van der waals heterostructures using inert shielding gas environment," *Applied Surface Science*, vol. 639, p. 158186, 08 2023.

[12] A. Raja, A. Chaves, J. Yu, G. Arefe, H. Hill, A. Rigosi, T. Berkelbach, P. Nagler, C. Schüller, T. Korn, C. Nuckolls, J. Hone, L. Brus, T. Heinz, D. Reichman, and A. Chernikov, "Coulomb engineering of the bandgap and excitons in two-dimensional materials," *Nature Communications*, vol. 8, p. 15251, 05 2017.

[13] M. Brahma, M. Van de Put, E. Chen, M. Fischetti, and W. Vandenberghe, "The importance of the image forces and dielectric environment in modeling contacts to two-dimensional materials," *npj 2D Materials and Applications*, vol. 7, 03 2023.

[14] J. Ryou, Y.-S. Kim, S. Kc, and K. Cho, "Monolayer mos2 bandgap modulation by dielectric environments and tunable bandgap transistors," *Scientific reports*, vol. 6, p. 29184, 07 2016.

[15] N. S. Rytova, "Screened potential of a point charge in a thin film," *Proc. MSU, Phys.*, 06 1967.

[16] L. V. Keldysh, "Coulomb interaction in thin semiconductor and semimetal films," *Soviet Journal of Experimental and Theoretical Physics Letters*, vol. 29, p. 716, 1979.

[17] M. Kumagai and T. Takagahara, "Excitonic and nonlinear-optical properties of dielectric quantum-well structures," *Physical review. B, Condensed matter*, vol. 40, pp. 12359–12381, 01 1990.

[18] E. Hanamura, N. Nagaosa, M. Kumagai, and T. Takagahara, "Quantum wells with enhanced exciton effects and optical non-linearity," *Materials Science and Engineering B-advanced Functional Solid-state Materials*, vol. 1, pp. 255–258, 12 1988.

[19] G. Gupta, S. Kallatt, and K. Majumdar, "Direct observation of giant binding energy modulation of exciton complexes in monolayer mose 2," *Physical Review B*, vol. 96, 03 2017.

[20] R. Salzwedel, L. Greten, S. Schmidt, S. Hughes, A. Knorr, and M. Selig, "Spatial exciton localization at interfaces of metal nanoparticles and atomically thin semiconductors," *Physical Review B*, vol. 109, 01 2024.

[21] D. Kleinman and R. Miller, "Band-gap renormalization in semiconductor quantum wells containing carriers," *Physical review. B, Condensed matter*, vol. 32, pp. 2266–2272, 09 1985.

[22] S. Das Sarma, R. Jalabert, and S. Yang, "Band-gap renormalization in semiconductor quantum wells.," *Physical review. B, Condensed matter*, vol. 41, pp. 8288–8294, 05 1990.

[23] A. Rodina and A. Efros, "Effect of dielectric confinement on optical properties of colloidal nanostructures," *Journal of Experimental and Theoretical Physics*, vol. 122, pp. 554–566, 03 2016.

[24] P.-Y. Lo, G.-H. Peng, W.-H. Li, Y. Yang, and S.-J. Cheng, "Full-zone valley polarization landscape of finite-momentum exciton in transition metal dichalcogenide monolayers," *Phys. Rev. Res.*, vol. 3, p. 043198, Dec 2021.

[25] G.-H. Peng, O. J. G. Sanchez, W.-H. Li, P.-Y. Lo, and S.-J. Cheng, "Tailoring the superposition of finite-momentum valley exciton states in transition-metal dichalcogenide monolayers by using polarized twisted light," *Phys. Rev. B*, vol. 106, p. 155304, Oct 2022.

[26] T. Zhu, C. Zheng, L. Xu, and M. Yang, "Exciton dissociation in two-dimensional transition metal dichalcogenides: Excited states and substrate effects," *Physical Review B*, vol. 110, 10 2024.

[27] Y. Tian, Q. Liu, Y. Ma, N. Wang, and Y. Gu, "Dielectric resonances of the cylindrical micro/nano cavity within epsilon-near-zero materials," *Optics Express*, vol. 31, 10 2023.

[28] K. Shenton, D. Bowler, and W. L. Cheah, "Influence of crystal structure on charge carrier effective masses in bifeo3," *Physical Review B*, vol. 100, 04 2018.

[29] W.-H. Li, J.-D. Lin, P.-Y. Lo, G.-H. Peng, C.-Y. Hei, S.-Y. Chen, and S.-J. Cheng, "The key role of non-local screening in the environment-insensitive exciton fine structures of transition-metal dichalcogenide monolayers," *Nanomaterials*, vol. 13, no. 11, 2023.

[30] M. Capizzi, S. Modesti, A. Frova, J. Staehli, M. Guzzi, and R. Logan, "Electron-hole plasma in direct-gap ga1-xalx as and k-selection rule," *Physical Review B*, vol. 29, pp. 2028–2035, 02 1984.

[31] Y. Onishi and L. Fu, "Universal relation between energy gap and dielectric constant," *Physical Review B*, vol. 110, 10 2024.

[32] J. Sans, J. F. Sánchez Royo, and A. Segura, "Study of the bandgap renormalization in ga-doped zno films by means of optical absorption under high pressure and photoelectron spectroscopy," *Superlattices and Microstructures - SUPERLATTICE MICROSTRUCT*, vol. 43, pp. 362–367, 04 2008.

[33] L. Gil and G. L. Lippi, "Phase instabilities in semiconductor lasers: A codimension-2 analysis," *Physical Review A*, vol. 90, 11 2014.

[34] T. Dinh Van, M. Yang, and H. Dery, "The coulomb interaction in monolayer transition-metal dichalcogenides," *Physical Review B*, vol. 98, 09 2018.

[35] Z. Lebens-Higgins, D. Scanlon, H. Paik, S. Sallis, Y. Nie, M. Uchida, N. Quackenbush, M. Wahila, G. Sterbinsky, D. Arena, J. Woicik, D. Schlom, and L. Piper, "Direct observation of electrostatically driven band gap renormalization in a degenerate perovskite transparent conducting oxide," *Phys. Rev. Lett.*, vol. 116, p. 027602, 01 2016.

[36] M. Ugeda, A. Bradley, S.-F. Shi, F. Da Jornada, Y. Zhang, D. Qiu, S.-K. Mo, Z. Hussain, Z.-X. Shen, F. Wang, S. Louie, and M. Crommie, "Giant bandgap renormalization and excitonic effects in a monolayer transition metal dichalcogenide semiconductor," *Nature materials*, vol. 13, 04 2014.

[37] T. C. Berkelbach, M. S. Hybertsen, and D. R. Reichman, "Theory of neutral and charged excitons in monolayer transition metal dichalcogenides," *Phys. Rev. B*, vol. 88, p. 045318, Jul 2013.

[38] A. Laturia, M. Van de Put, and W. Vandenberghe, "Dielectric properties of hexagonal boron nitride and transition metal dichalcogenides: from monolayer to bulk," *npj 2D Materials and Applications*, vol. 2, 03 2018.

[39] J. L. Rosenholtz and D. T. Smith, "The dielectric constant of mineral powders," *American Mineralogist: Journal of Earth and Planetary Materials*, vol. 21, no. 2, pp. 115–120, 1936.

[40] A. Maruvada, K. Shubhakar, N. Raghavan, K. Pey, and S. O'Shea, "Dielectric breakdown of 2d muscovite mica," *Scientific Reports*, vol. 12, 08 2022.

[41] J. Robertson, "High dielectric constant oxides," *European Physical Journal-applied Physics*, vol. 28, no. 3, pp. 265–291, 2004.

[42] J. Liu, M. Okamura, H. Mashiko, M. Imura, M. Liao, R. Kikuchi, M. Suzuka, and Y. Koide, "Experimental formation and mechanism study for super-high dielectric constant alox/tioy nanolaminates," *Nanomaterials*, vol. 13, p. 1256, 04 2023.

[43] C. Inc., "Comsol," 2020.

[44] H. Y. Ramírez and A. Santana, "Two interacting electrons confined in a 3d parabolic cylindrically symmetric potential, in presence of axial magnetic field: A finite element approach," *Computer Physics Communications*, vol. 183, no. 8, pp. 1654–1657, 2012.

[45] N. R. Fino, A. S. Camacho, and H. Y. Ramírez, "Coupling effects on photoluminescence of exciton states in asymmetric quantum dot molecules," *Nanoscale Research Letters*, vol. 9, p. 297, Jun 2014.

[46] M. Zapata-Herrera, Ángela S. Camacho, and H. Y. Ramírez, "Influence of the confinement potential on the size-dependent optical response of metallic nanometric particles," *Computer Physics Communications*, vol. 227, pp. 1–7, 2018.

[47] K. K. Kam and B. A. Parkinson, "Detailed photocurrent spectroscopy of the semiconducting group vib transition metal dichalcogenides," *The Journal of Physical Chemistry*, vol. 86, pp. 463–467, Feb 1982.

[48] J. A. Baglio, G. S. Calabrese, E. Kamieniecki, R. Kershaw, C. P. Kubiak, A. J. Ricco, A. Wold, M. S. Wrighton, and G. D. Zoski, "Characterization of n-type semiconducting tungsten disulfide photoanodes in aqueous and nonaqueous electrolyte solutions: Photo-oxidation of halides with high efficiency," *Journal of The Electrochemical Society*, vol. 129, p. 1461, jul 1982.

[49] H. Ramirez, A. Camacho, and L. Lew Yan Voon, "Dc electric field effects on the electron dynamics in double rectangular quantum dots," *Brazilian Journal of Physics*, vol. 36, pp. 869–873, 2006.

[50] H. Y. Ramirez, A. S. Camacho, and L. C. L. Y. Voon, "Influence of shape and electric field on electron relaxation and coherent response in quantum-dot molecules," *Journal of Physics: Condensed Matter*, vol. 19, p. 346216, jul 2007.

[51] A. H. Rodríguez and H. Y. Ramírez, "Analytical calculation of eigen-energies for lens-shaped quantum dot with finite barriers," *The European Physical Journal B*, vol. 66, pp. 235–238, Nov 2008.

[52] T. A. Welsch and M. F. Doty, "Pbs/cds core/shell quantum dots designed to enable efficient photon upconversion for solar energy applications," *ACS Applied Optical Materials*, vol. 2, pp. 2184–2195, Oct 2024.